DOI: 10.13208/j.electrochem.131178 **Artical ID**:1006-3471(2014)05-0401-09
Cite this: *J. Electrochem.* **2014**, *20*(5): 401-409 **Http**://electrochem.xmu.edu.cn

Boosting Electrocatalytic Activity of Nitrogen-Doped Graphene/Carbon Nanotube Composite for Oxygen Reduction Reaction

ZHANG Yun[1,2], HU Jin-song[1*], JIANG Wen-jie[1,2], GUO Lin[1,2],
WEI Zi-dong[2*], WAN Li-jun[1]

(1. *Beijing National Laboratory for Molecular Sciences, Key Laboratory of Molecular Nanostructure and Nanotechnology, Institute of Chemistry, Chinese Academy of Sciences, Beijing* 100190, *China*;
2. *State Key Laboratory of Power Transmission Equipment & System Security and New Technology, College of Chemistry and Chemical Engineering, Chongqing University, Chongqing* 400044, *China*)

Abstract: Developing low-cost catalysts with high electrocatalytic activity for oxygen reduction reaction (ORR) has recently attracted much attention because the sluggish ORR currently limits the performance and commercialization of fuel cells and metal-air batteries as well. Nitrogen doped carbon materials have been considered as promising candidates for the replacement of high-cost and scarce Pt-based catalysts although their electrocatalytic activity still needs to be much improved. In this work, an improved nitrogen-doped graphene/carbon nanotubes composite (N-rGO/CNT) was developed as an efficient ORR electrocatalyst. It was found that the ORR activity of N-rGO/CNT composite could be significantly enhanced by introducing iron in nitrogen-doping process, and further boosted by constructing nanopores in the catalyst for allowing more catalytically active sites accessible and enhancing mass transfer. Moreover, the electrochemical measurement showed that the improved catalysts exhibited superior tolerance to methanol crossover and good durability, indicating their potential as ORR catalysts for energy conversion and storage applications.

Key words: graphene; carbon nanotubes; electrocatalysts; oxygen reduction reaction; mesoporous
CLC Number: O911.42 **Document Code**: A

The oxygen reduction reaction (ORR) is an important process in energy conversion and storage devices such as fuel cells and metal-air batteries[1-2]. Pt and its alloys are well known as most efficient catalysts for ORR[3-4], but their sluggish kinetics in ORR, high price, limit supply, and poor durability impede the development and commercialization of these devices. Nowadays, tremendous effort has been geared towards developing non-platinum-group-metal (non-PGM) catalysts for ORR in view of low cost and better durability and tolerance to fuel crossover. In general, there are three types of non-PGM materials. First one is macrocyclic metal-N_4 complexes, containing single macrocycle[5], cofacial macrocycle-based dimmers[6], and their derivatives[7]. Second one is carbon materials doped with heteroatoms (such as N[8-9], P[10], S[11], Se[12], B[13], and F[14]), including dual-doped[15] and trinary-doped[16] carbon materials. The last is the materials based on transition metals, such as transition met al chalcogenide[17], transition metal nitride[18-19], and transition metal or metal oxide supported on nitrogen-doped carbon materials[20-21].

No matter what type of catalyst will be used, to be viable, its activity should at least approach that of

Received: 2014-03-13, Revised: 2014-04-23 *Corresponding author, Tel: (86-10) 82613929, E-mail: hujs@iccas.ac.cn, zdwei@cqu.edu.cn

This work was supported by the National Natural Science Foundation of China (Grants Nos. 91127044, 21173237, and 21121063), the National Key Project on Basic Research (Grants Nos. 2011CB808700 and 2012CB215500), and the Chinese Academy of Sciences

traditional but more expensive Pt/C catalysts. Among various materials, N-doped carbon materials, including N-doped graphene (usually referred to as reduced graphene oxide, N-rGO), N-doped carbon nanotubes (N-CNT) and their composites (N-rGO-CNT), have attracted much attention[8,22-23]. In linear sweep voltammetry (LSV) measurements, N-rGO often exhibited more positive on-set potential (close to that of Pt/C catalysts) owing to more catalytically active sites, but inferior half-wave potential and current density caused by the insufficient conductivity and mass transfer due to incomplete reduction and stacking of graphene sheets. N-CNT commonly showed insufficient electrocatalytic activity for ORR but held the merits of good conductivity and mass transfer. Taking in account these facts, N-rGO-CNT prepared via several methods were reported and they exhibited reasonable catalytic activity and durability for ORR[12,23-24], although their activities still need to be much improved. On the other hand, N-doped porous carbon materials allowed more active sites to engage in ORR due to large surface area, and thus demonstrated enhanced ORR catalytic activity[25]. However, the activities of these porous catalysts are still much lower than that of Pt-based catalysts despite tremendous efforts have been made. The main reason could be attributed to poor electron conductivity caused by heavy heteroatom doping and porous structures.

In consideration of these situations, we reported here a porous nitrogen-doped graphene/carbon nanotubes composite with enhanced electrocatalytic performance for ORR by boosting the activity of N-rGO-CNT via the introduction of iron and the construction of nanopores in the catalyst. By taking advantage of high conductivity from carbon nanotubes network and high activity from doped graphene, and further integrating the merits of more accessible catalytically active sites and easy mass transfer from mesoporous structures, the modified composite exhibited excellent electrocatalytic performance for ORR in terms of high activity and superior tolerance to methanol crossover with good durability.

1 Experimental

1.1 Synthesis of Materials

The graphene oxide (GO) was prepared with the modified Hummers method [26]. Carbon nanotubes (CNT, Shenzhen Nanotech Port Co. Ltd.) were refluxed in concentrated nitric acid at 80 ℃ for 3 h to remove impurities.

1) Synthesis of Fe-N-rGO-CNT

40 mg pretreated CNT, 10 mg sodium dodecyl sulfate (SDS, Sinopharm Chemical Reagent Co., Ltd.), and 51.1 mg $Fe(NO_3)_3 \cdot 9H_2O$ (Sigma-Aldrich) were ultrasonically dispersed in 36.923 mL aqueous solution for 1 h. 3.077 mL GO suspension (2.6 mg·mL^{-1}) was added into above solution and sonicated for another hour. The obtained suspension was then transferred into an autoclave with 50 mL Teflon liner and heated at 180 ℃ for 12 h. The product was filtered, washed with water and ethanol, and then dried overnight at 80 ℃. After that, the product and melamine (nitrogen source, Sigma-Aldrich) in a weight ratio of 1∶10 were mixed together and ground for about 15 min, followed by a heat-treatment at 900 ℃ in argon atmosphere for 1 h at a heating ramping rate of 5 ℃·min^{-1}.

2) Synthesis of porous Fe-N-rGO-CNT (*p*-Fe-N-rGO-CNT)

Porous Fe-N-rGO-CNT was prepared in parallel as that for Fe-N-rGO-CNT, except for adding 0.277 mL colloidal silica (Ludox HS-40, Sigma-Aldrich) during the preparation of CNT suspension and etching away silica with 10% HF acid after heat-treatment. The weight ratio of colloidal silica/(GO+CNT) was 3∶1 in a typical process.

3) Synthesis of N-rGO-CNT

N-rGO-CNT was prepared as a reference sample in parallel with that for Fe-N-rGO-CNT except for no addition of iron source during the preparation of CNT suspension.

1.2 Characterization

The morphology and composition of as-prepared samples were first investigated by using scanning electron microscope (SEM, Hitachi S-4800, Japan) operated at 15 kV and transmission electron microscopy JEM-2100F (TEM, JEM-2100F, JEOL,

Japan) equipped with energy dispersive X-ray spectroscopy (EDS) analytical system. X-ray photoelectron spectroscopy (XPS) measurements were carried out on a VG ESCALab220i-XL using a monochromic Mg K_{α} source. Quantachrome Autosorb AS-1 was used to record nitrogen adsorption-desorption isotherms at 77 K. The samples were degassed in a vacuum at 150 ℃ for at least 6 h before measurement.

1.3 Electrochemical Tests

All electrochemical experiments were performed on a rotating ring-disk electrode rotator (RRDE-3A, ALS, Japan) connected to an electrochemical workstation (CHI 760E, ChenHua, Shanghai, China) at room temperature. The three electrode cell system was used, which consisted of a working electrode (glassy carbon rotating electrode (RDE), 3 mm in diameter) loaded with catalyst, a reference electrode (3 mol·L^{-1} KCl Ag/AgCl, ALS, Japan), and a counter electrode (platinum foil). The working electrode was prepared by pasting catalyst ink on RDE. In brief, a homogeneous ink was formed by dispersing 2 mg catalyst in 800 μL ethanol under ultrasonication. 17 μL ink was dropped onto freshly polished GC electrode, yielding an catalyst loading of 600 μg·cm^{-2}. After drying in air, 2 μL nafion (0.5%, by mass) solution was covered onto catalyst surface. After drying in air, the working electrode was ready for test. The commercial Pt/C (20% Pt loading, by mass, Johnson Matthey (JM)) was used for comparison. Pt loading was 25.5 μg·cm^{-2}.

The H_2O_2 yield was measured on a rotating ring-disk electrode (RRDE) with a disk diameter of 4 mm at a catalyst loading of 600 μg·cm^{-2}. Four-electron selectivity of catalyst was evaluated based on H_2O_2 yield, which was calculated from the following equation:

$$H_2O_2(\%) = 200 \times \frac{I_R/N}{(I_R/N)+I_D} \quad (1)$$

The electron transfer number (n) was calculated from the following equation:

$$n = 4 \times \frac{I_D}{(I_R/N) + I_D} \quad (2)$$

where, I_D and I_R are the disk and ring currents, respectively; N is the ring collection efficiency and equals to 0.424.

2 Results and Discussion

The electrocatalytic performances of N-rGO-CNT, Fe-N-rGO-CNT, p-Fe-N-rGO-CNT, and reference Pt/C electrodes were first evaluated by linear sweep voltammetry (LSV) technique. LSV polarization curves were recorded on RDE in 0.1 mol·L^{-1} O_2-saturated KOH electrolyte at a rotation speed of 1600 r·min^{-1} and a scan rate of 10 mV·s^{-1}. As seen in Fig. 1, the on-set potential and half-wave potential of N-rGO-CNT were much more negative than others, indicating a much inferior performance for catalyzing ORR. However, after introducing iron into composite in N-rGO-CNT, the electrocatalytic performance of Fe-N-rGO-CNT for ORR was improved by positively shifting the on-set potential and half-wave potential. Moreover, after introducing porous structure in Fe-N-rGO-CNT, the electrocatalytic activity of p-Fe-N-rGO-CNT was further boosted. The half-wave potential was positively shifted to -0.187 V (vs. Ag/AgCl) in p-Fe-N-rGO-CNT, which are 96 mV and 31 mV positive than those of N-rGO-CNT and Fe-N-rGO-CNT, respectively, and only 37 mV negative than that of Pt/C catalyst. The limiting current density of p-Fe-N-rGO-CNT was also much enhanced over the whole potential range compared to that of two other analogues and became close to the level of Pt/C. These results showed that the introduction of porous structure significantly boosted the electrocatalytic performance of the composite.

The morphology and composition of p-Fe-N-rGO-CNT were subsequently examined by SEM and TEM. It can be seen from a typical SEM image (Fig. 2A) that the composite was comprised of one dimensional nanostructure and sheet-like structures which are in close contact. TEM observation (Fig. 2B) clearly revealed that the typical nanotube-like feature from CNT as well as very thin layers and wrinkled folds which are typical features of graphene layers. These results unarguably confirmed that p-Fe-N-rGO-CNT consisted of graphene and CNT. It was also seen that these graphene layers were in a very loose status in

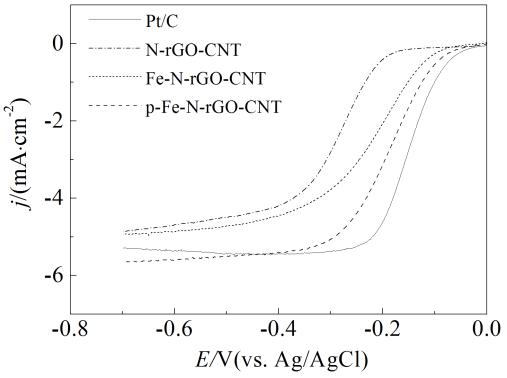

Fig. 1 LSV curves of different catalysts recorded in 0.1 mol·L^{-1} O_2-saturated KOH at a scan rate of 10 mV·s^{-1} and a rotation speed of 1600 r·min^{-1}

stead of close stacking and CNT intercalated in these layers. High resolution TEM (HRTEM) was used to further investigate the microstructure of the material. HRTEM image shown in Fig. 2C displayed that a number of nanopores existed on the grapheme layers. Fig 2D presents a typical HRTEM image of a nanoparticle in dark, contrast in Fig. 2B. It clearly exhibited the lattice fringes with a d spacing of 0.203 nm, corresponding to the interplanar distance of (110) planes of metallic Fe. Energy dispersive X-ray spectroscopy (EDS) measurements also evidenced the existence of element iron and nitrogen (Fig. 2E). The signal of element copper in Fig. 2E should be from copper grid used for TEM observation.

The surface area and porosity of *p*-Fe-N-rGO-CNT were further investigated by nitrogen isothermal adsorption-desoption technique. The adsorption-desorption isotherm shown in Fig. 3A present a typical feature of mesoporou materials. The total specific surface area on the basis of Brunauer-Emmett-Teller (BET) analysis for *p*-Fe-N-rGO-CNT is 97.55 m^2·g^{-1}, which is larger than 55.61 m^2·g^{-1} for Fe-N-rGO-CNT (Tab. 1). Fig. 3B shows the corresponding Barrett-Joyner-Halenda (BJH) pore size distribution analysis, which indicated that the material had bimodal pore size distribution centered around 4 nm and 30 nm. The increase in BET surface area can be ascribed to the formation of porous structure by thermal treating with silica and subsequent removal of silica[15]. The existence of silica during thermal treatment

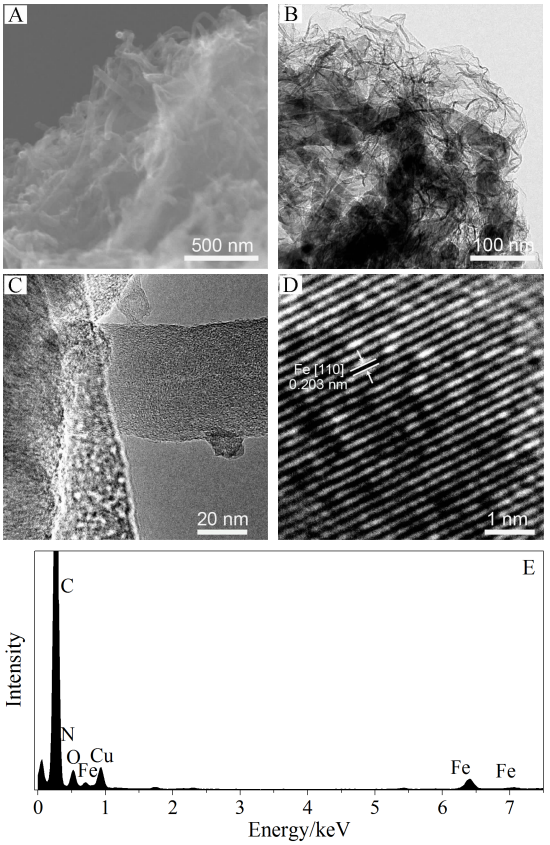

Fig. 2 Typical SEM image (A) and TEM images (B, C) of *p*-Fe-N-rGO-CNT, HRTEM image (D) of iron particle and EDS spectrum (E) of *p*-Fe-N-rGO-CNT

and N-doping process would introduce more defects in graphene/CNT, which provided more high-energy edges as active sites for ORR [15]. The porous structure was also believed to allow more catalytically active sites accessible for oxygen molecules and favor the mass transfer during ORR.

In order to further understanding the enhancement in electrocatalytic activity of *p*-Fe-N-rGO-CNT, XPS spectra were recorded for both Fe-N-rGO-CNT and *p*-Fe-N-rGO-CNT. As shown in Fig. 4A and B, both samples showed obvious nitrogen signals, proving the successful introduction of nitrogen. The total nitrogen contents were calculated to be 5.07% for Fe-N-rGO-CNT and 4.02% for *p*-Fe-N-rGO-CNT. The slight decrease in nitrogen content in the latter could be due to the possible reaction between nitrogen species and silica during heating treatment followed by the removal process with HF. Moreover, the high-resolution N1s signals in two XPS spectra

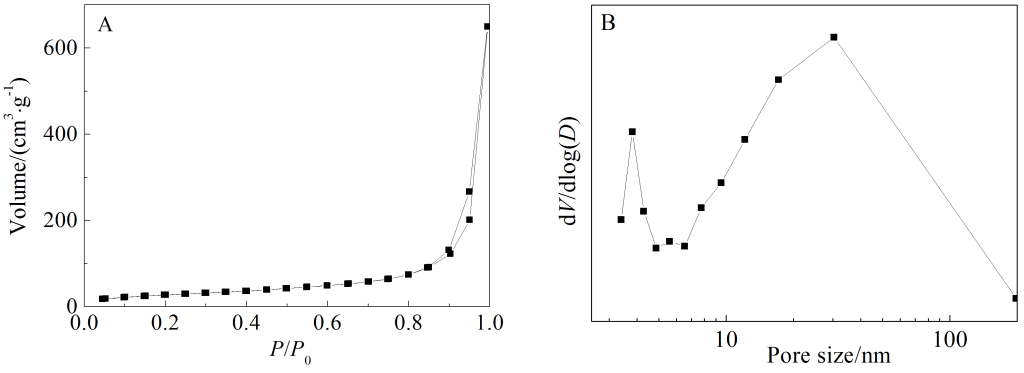

Fig. 3　N_2 adsorption-desorption isotherm (A) and BJH pore size distribution plot (B) of *p*-Fe-N-rGO-CNT

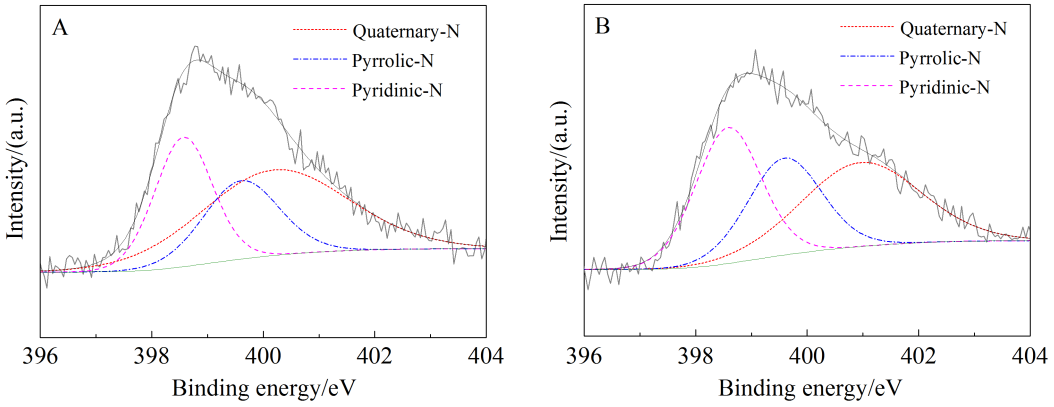

Fig. 4　High-resolution N1s peaks in XPS spectra of Fe-N-rGO-CNT (A) and *p*-Fe-N-rGO-CNT (B)
The peaks were deconvoluted into three typical types of nitrogen species

Tab. 1　BET surface areas and nitrogen contents calculated from XPS spectra of Fe-N-rGO-CNT and *p*-Fe-N-rGO-CNT

Sample	Surface area/(m^2·g^{-1})	Total N content/%	Pyridinic-N%	Pyrrolic-N/%	Quaternary-N/%
Fe-N-rGO-CNT	55.61	5.07	28.67	22.80	48.53
p-Fe-N-rGO-CNT	97.55	4.02	34.11	27.46	38.43

were deconvoluted into three typical components of nitrogen species, pyridinic type (~ 398.58 eV), pyrrolic type (~ 399.60 eV), and quaternary type (~ 400.96 eV) nitrogen, to further investigate the bonding state of doped nitrogen. It can be seen that two samples embodied similar nitrogen components. The quantitative analysis result of each type of nitrogen was summarized in Tab. 1. In both cases, pyridinic-N and quaternary-N were dominated in the catalysts. It could be concluded that the slight difference in nitrogen contents and bonding states will not be responsible for the differences in electrocatalytic performance between *p*-Fe-N-rGO-CNT and Fe-N-rGO-CNT, given that even less nitrogen content in the former and similar components of nitrogen species are presented in both catalysts. Therefore, taking into account the above structural characterization and BET analysis, the better electrocatalytic performance achieved in *p*-Fe-N-rGO-CNT should be mainly attributed to the porous structure and higher surface area.

Moreover, to further explore how colloidal silica influenced the formation of active sites, we prepared p-Fe-N-rGO-CNT with different amounts of colloidal silica. Fig. 5A shows the polarization curves of these composites recorded in RDE measurements. It could be seen that when the weight ratio of colloidal silica/

(GO+CNT) was increased from 1∶1 to 3∶1, the on-set potential and half-wave potential of polarization curve were positively shifted, indicating the improvement of electrocatalytic activity. Adding more silica (5∶1) did not achieve further improvement. Therefore, the ratio of 3∶1 was used in the above discussion. On the other hand, it was found that the amount of iron also affected the performance of the catalysts. As shown in Fig. 5B, when the amount of iron was raised from 5% to 10%, the activity of catalyst was obviously promoted in terms of 32 mV positive shift of half-wave potential; while the amount of iron was further increased to 15%, the ORR activity of catalyst did not change much with a only very slight increase in current density. Besides, it should be noted that the ratio of rGO and CNT in the composites influenced their electrocatalytic activity as well. The optimal weight ratio of rGO and CNT was found to be 0.2 and used in the preparation of all composites in this work.

The selectivity of four-electron reduction of oxygen was explored by using RRDE to further evaluate the performance of present *p*-Fe-N-rGO-CNT composite for ORR. In the RRDE measurement, the potential of Pt ring electrode was set to 0.5 V for detecting peroxide species forming on disc electrode. As seen in Fig. 6A, the H_2O_2 yield in ORR remained below 7.5% at all potentials, corresponding to an electron transfer number of ~ 3.9 in ORR. It suggested that *p*-Fe-N-rGO-CNT exhibited high efficient and beneficial four-electron oxygen reduction process in catalyzing ORR, similar to commercial Pt/C catalyst.

Considering fuel crossover often happens in fuel cells and severely deteriorates the performance of cathode catalyst, a practical cathode catalyst should have excellent tolerance to fuel. Therefore, the electrocatalytic performance of present *p*-Fe-N-rGO-CNT catalyst was also examined in the presence or absence of methanol, a representative fuel in direct methanol fuel cells, and compared to that of commercial Pt/C catalyst. The results showed that the existence of methanol did not influence the electrocatalytic activity of *p*-Fe-N-rGO-CNT as indicated by unchanged LSV curves (Fig. 6B), but significantly deteriorated the performance of Pt/C catalyst in view of a negative shift in half-wave potential of 185 mV in LSV curves (Fig. 6C). Furthermore, the durability of *p*-Fe-N-rGO-CNT was also evaluated via chronoamperometric measurements and compared to that of Pt/C catalyst. Fig. 6D displayed that Pt/C suffered from around 40% current loss, while *p*-Fe-N-rGO-CNT only lost less 20% current after 10000 s recording. These results indicated that the present *p*-Fe-N-rGO-CNT catalyst demonstrated a superior tolerance to fuel crossover and durability.

3 Conclusions

In summary, a porous nitrogen-doped graphene/carbon nanotubes composite (*p*-Fe-N-rGO/CNT) was

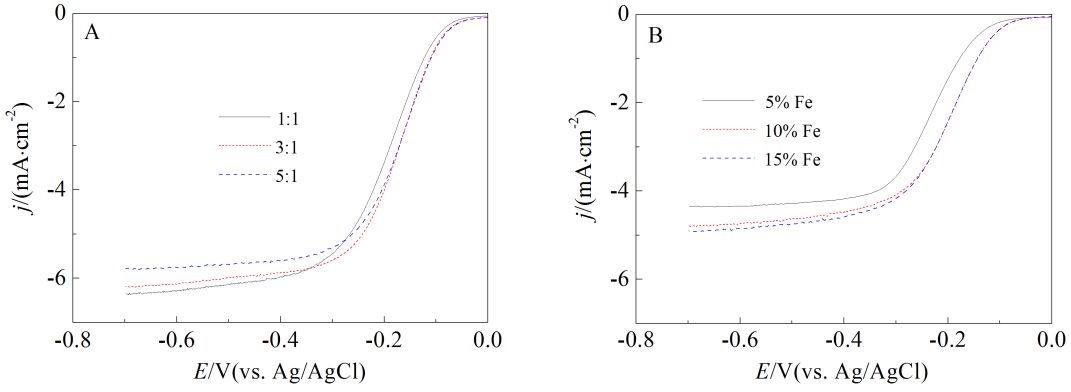

Fig. 5 LSV curves of *p*-Fe-N-rGO-CNT prepared at different weight ratios of silica/(GO+CNT) (A) and Fe-N-rGO-CNT prepared at different amounts of iron source (B)

All curves were recorded in 0.1 mol·L^{-1} O_2-saturated KOH at a scan rate of 10 mV·s^{-1} and a rotation speed of 1600 r·min^{-1}

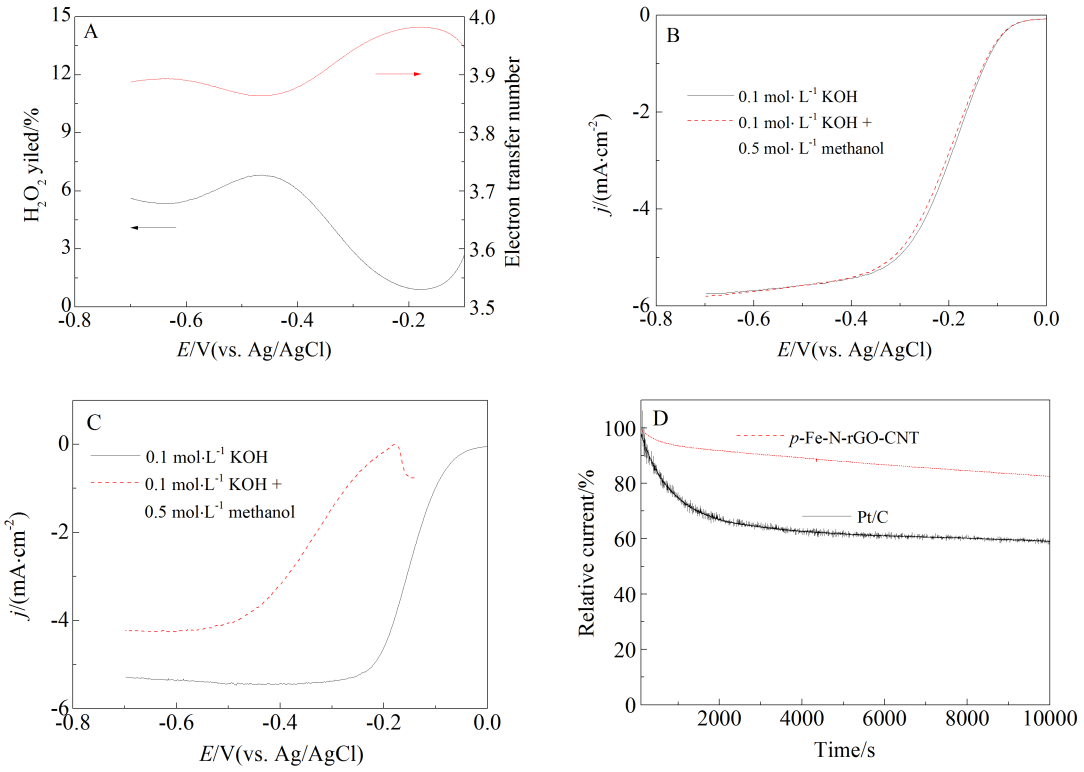

Fig. 6 H_2O_2 yield and electron-transfer number in RRDE measurement of *p*-Fe-N-rGO-CNT (A), LSV curves of *p*-Fe-N-rGO-CNT (B), LSV curves of Pt/C (C) recorded in the presence or absence of 0.5 mol·L^{-1} methanol, and current-time (*i-t*) chronoamperometric responses of *p*-Fe-N-rGO-CNT and Pt/C recorded at -0.2 V in 0.1 mol·L^{-1} O_2-saturated KOH (D)

developed as an electrocatalyst for ORR. It was found that the introduction of iron and porous structure significantly boosted the electrocatalytic activity of N-rGO/CNT. The possible reasons for this improvement and the influence of experimental conditions on the performance of catalysts were discussed. The electrochemical results suggested that the present *p*-Fe-N-rGO/CNT exhibited excellent electrocatalytic activity for ORR, as well as better durability and tolerance to methanol in comparison with commercial Pt/C. The design idea described here could be extended to synthesize other similar catalysts in a cost-effective and scalable way for wide applications.

Acknowledgements

We gratefully thank the supports from the National Natural Science Foundation of China (Grants Nos. 91127044, 21173237, and 21121063), the National Key Project on Basic Research (Grants Nos. 2011CB808700 and 2012CB215500), and the Chinese Academy of Sciences.

References:

[1] Wu G, Zelenay P. Nanostructured nonprecious metal catalysts for oxygen reduction reaction[J]. Accounts of Chemical Research, 2013, 46(8): 1878-1889.

[2] Thackeray M M, Chan M K Y, Trahey L, et al. Vision for designing high-energy, hybrid Li ion/Li-O_2 cells[J]. The Journal of Physical Chemistry Letters, 2013, 4 (21): 3607-3611.

[3] Stamenkovic V R, Fowler B, Mun B S, et al. Improved oxygen reduction activity on $Pt_3Ni(111)$ via increased sur face site availability[J]. Science, 2007, 315(5811): 493-497.

[4] Lim B, Jiang M, Camargo P H C, et al. Pd-Pt bimetallic nanodendrites with high activity for oxygen reduction[J]. Science, 2009, 324(5932): 1302-1305.

[5] Liu R, von Malotki C, Arnold L, et al. Triangular trinuclear metal-N_4 complexes with high electrocatalytic activity for oxygen reduction[J]. Journal of the American Chemical Society, 2011, 133(27): 10372-10375.

[6] Chang C J, Loh Z-H, Shi C, et al. Targeted proton delivery in the catalyzed reduction of oxygen to water by bimetallic pacman porphyrins[J]. Journal of the American Chemical Society, 2004, 126(32): 10013-10020.

[7] Kadish K M, Frémond L, Ou Z, et al. Cobalt(III) corroles as electrocatalysts for the reduction of dioxygen: Rctivity of a monocorrole, biscorroles, and porphyrin-corrole dyads [J]. Journal of the American Chemical Society, 2005, 127 (15): 5625-5631.

[8] Sheng Z, Shao L, Chen J, et al. Catalyst-free synthesis of nitrogen-doped graphene via thermal annealing graphite oxide with melamine and its excellent electrocatalysis [J]. ACS Nano, 2011, 5(6): 4350-4358.

[9] Wu L, Feng H, Liu M, et al. Graphene-based hollow spheres as efficient electrocatalysts for oxygen reduction[J]. Nanoscale, 2013, 5(22): 10839-10843.

[10] Zhang C, Mahmood N, Yin H, et al. Synthesis of phosphorus-doped graphene and its multifunctional applications for oxygen reduction reaction and lithium ion batteries[J]. Advanced Materials, 2013, 25(35): 4932-4937.

[11] Yang Z, Yao Z, Li G, et al. Sulfur-doped graphene as an efficient metal-free cathode catalyst for oxygen reduction [J]. ACS Nano, 2011, 6(1): 205-211.

[12] Jin Z, Nie H, Yang Z, et al. Metal-free selenium doped carbon nanotube/graphene networks as a synergistically improved cathode catalyst for oxygen reduction reaction [J]. Nanoscale, 2012, 4(20): 6455-6460.

[13] Wang S, Zhang L, Xia Z, et al. BCN graphene as efficient metal-free electrocatalyst for the oxygen reduction reaction[J]. Angewandte Chemie International Edition, 2012, 51(17): 4209-4212.

[14] Sun X, Zhang Y, Song P, et al. Fluorine-doped carbon blacks: Highly efficient metal-free electrocatalysts for oxygen reduction reaction[J]. ACS Catalysis, 2013, 3(8): 1726-1729.

[15] Liang J, Jiao Y, Jaroniec M, et al. Sulfur and nitrogen dual-doped mesoporous graphene electrocatalyst for oxygen reduction with synergistically enhanced performance [J]. Angewandte Chemie International Edition, 2012, 51(46): 11496-11500.

[16] Choi C H, Park S H, Woo S I. Binary and ternary doping of nitrogen, boron, and phosphorus into carbon for enhancing electrochemical oxygen reduction activity [J]. ACS Nano, 2012, 6(8): 7084-7091.

[17] Wang H, Liang Y, Li Y, et al. $Co_{1-x}S$-graphene hybrid: A high-performance metal chalcogenide electrocatalyst for oxygen reduction [J]. Angewandte Chemie International Edition, 2011, 50(46): 10969-10972.

[18] Cui Z, Burns R G, DiSalvo F J. Mesoporous $Ti_{0.5}Nb_{0.5}N$ ternary nitride as a novel noncarbon support for oxygen reduction reaction in acid and alkaline electrolytes [J]. Chemistry of Materials, 2013, 25(19): 3782-3784.

[19] Liu M, Dong Y, Wu Y, et al. Titanium nitride nanocrystals on nitrogen-doped graphene as an efficient electro catalyst for oxygen reduction reaction [J]. Chemistry-A European Journal, 2013, 19(44): 14781-14786.

[20] Wu G, More K L, Johnston C M, et al. High-performance electrocatalysts for oxygen reduction derived from polyaniline, iron, and cobalt[J]. Science, 2011, 332(6028): 443-447.

[21] Wu Z S, Yang S, Sun Y, et al. 3D nitrogen-doped graphene aerogel-supported Fe_3O_4 nanoparticles as efficient elec trocatalysts for the oxygen reduction reaction [J]. Journal of the American Chemical Society, 2012, 134 (22): 9082-9085.

[22] Gong K, Du F, Xia Z, et al. Nitrogen-doped carbon nanotube arrays with high electrocatalytic activity for oxygen reduction[J]. Science, 2009, 323(5915): 760-764.

[23] Chen P, Xiao T Y, Qian Y H, et al. A Nitrogen-doped graphene/carbon nanotube nanocomposite with synergis tically enhanced electrochemical activity [J]. Advanced Materials, 2013, 25(23): 3192-3196.

[24] Ma Y, Sun L, Huang W, et al. Three-dimensional nitrogen-doped carbon nanotubes/graphene structure used as a metal-free electrocatalyst for the oxygen reduction reac tion[J]. The Journal of Physical Chemistry C, 2011, 115 (50): 24592-24597.

[25] Yang W, Fellinger T P, Antonietti M. Efficient metal-free oxygen reduction in alkaline medium on high-surface-area mesoporous nitrogen-doped carbons made from ionic liquids and nucleobases[J]. Journal of the American Chemical Society, 2010, 133(2): 206-209.

[26] Hummers W S, Offeman R E. Preparation of graphitic oxide[J]. Journal of the American Chemical Society, 1958, 80(6): 1339-1339.

通过铁掺杂和造孔提高氮掺杂石墨烯/碳纳米管复合物电催化氧还原性能的研究

张　云[1,2], 胡劲松[1*], 江文杰[1,2], 郭　琳[1,2], 魏子栋[2*], 万立骏[1]

(1. 中国科学院化学研究所 中国科学院分子纳米结构与纳米技术重点实验室, 北京分子科学国家实验室,北京 100190;
2. 重庆大学 化学化工学院, 输配电装备及系统安全与新技术国家重点实验室, 重庆 400044)

摘要: 氧还原反应催化剂的性能直接影响着能源转换和存储器件如燃料电池和金属-空气电池的性能. 开发低成本、高性能的非铂族金属氧还原催化剂对于这类器件的实际应用和商业化十分重要, 因此备受关注. 氮掺杂的石墨烯 / 碳纳米管复合物同时具备碳纳米管的良好导电性能和有利于传质的三维网络结构优点,以及氮掺杂石墨烯的高活性优点,因此有望发展为这类可替代铂族催化剂的氧还原电催化剂之一,但目前其催化性能还需进一步提高. 本文研究发现通过在氮掺杂石墨烯 / 碳纳米管复合物的过程中引入铁元素可以有效提高催化剂的氧还原活性,并且发现通过在热处理和氮掺杂过程中加入二氧化硅纳米颗粒及随后除去二氧化硅,可以在氮掺杂的石墨烯/碳纳米管复合物材料中有效地形成多孔结构. 这种多孔结构的形成不仅可以在复合物中引入更多的高活性催化位点,而且有利于暴露更多的催化活性位并促进氧还原反应中的传质过程. 结合碳纳米管、石墨烯和多孔结构的三者优点,所制备的多孔氮掺杂碳材料表现出优异的电催化氧还原性能. 进一步的实验表明,这类材料还表现出优异的抗甲醇中毒能力和良好的稳定性,因此在性能改进后有望用于燃料电池等能量转换与存储器件.

关键词: 石墨烯; 碳纳米管; 电催化剂; 氧还原反应; 介孔材料